

We are IntechOpen, the world's leading publisher of Open Access books Built by scientists, for scientists

6,900

Open access books available

186,000

International authors and editors

200M

Downloads

Our authors are among the

154

Countries delivered to

TOP 1%

most cited scientists

12.2%

Contributors from top 500 universities



WEB OF SCIENCE™

Selection of our books indexed in the Book Citation Index
in Web of Science™ Core Collection (BKCI)

Interested in publishing with us?
Contact book.department@intechopen.com

Numbers displayed above are based on latest data collected.
For more information visit www.intechopen.com



Innovative “Green” Tribological Solutions for Clean Small Engines

Xana Fernández-Pérez, Amaya Igartua,
Roman Nevshupa, Patricio Zabala, Borja Zabala,
Rolf Luther, Flavia Gili and Claudio Genovesio

Additional information is available at the end of the chapter

<http://dx.doi.org/10.5772/55836>

1. Introduction

Since its invention in the last quarter of the nineteenth century and during all the twentieth century, two-stroke engines penetrated in many industrial, automotive and handheld applications where engines with high specific power, simple design, light overall weight and low cost are required. Presently, two-stroke engines are commonly used in motorcycles, scooters, chainsaw, agricultural machinery, railways grinding machines, outboard applications, etc.

Usually, the moving parts of a two-stroke motor are lubricated either by using mixture of oil with fuel or by pumping oil from a separate tank. Both designs use total-loss lubrication method, with the oil being burnt in the combustion chamber. Therefore, the lubricating oil must meet specific requirements: it must have an optimal balance of light and heavy oil components to lubricate at high temperature, it must produce no deposits (carbon sooty and other) on moving parts, and it should be ash-less. In addition, the oil should provide good protection of moving parts at high speed under deceleration of engine with the throttle closed, when the engine usually suffers from oil-starvation.

Also, two-stroke engine produce more contaminants than four-stroke engines, due to oil burning in the combustion chamber. Therefore, it is very important to reduce these contaminations to meet ecological requirements.

Most challenging issue of the European technological strategy resides in complete substitution of fossil-based fuels and lubricating oils with renewable eco-friendly and high performance materials. Esters and polyglycols were identified as alternative base oils because of their high biodegradability, low toxicity; low ash formation and absence of polymer compo-

nents, in [1]. Synthetic esters are characterized by their polar structure, high wear resistance, good viscosity-temperature behaviour, miscibility with non-fossil fuels. Esther-base oils can be blended with various components like antifoam agents, oxidation inhibitors, pour-point depressants, antirust agents, detergents, anti-wear agents, friction reducers, viscosity index improvers, etc., to create environmental friendly prototype engine oils and to meet the changing environmental requirements in low sulphur fuels and other alternative fuels and their application to engine oils.

Low metal additives content and clean-burnt characteristics result in less engine fouling with much reduced ring stick and lower levels of dirt built-up on ring grooves, skirts and under crowns. Owing to the presence of polar ester groups in the molecule which have higher adhesion to metal surface, esters have much better lubricity than hydrocarbons. The performance of the ester-based lubricating oils can be further improved by selecting a proper base oil and additive package.

Another important problem is related with performance of fuel injector system when bio fuels are used. Diesel injection nozzles consist of a body (usually in Ni-Cr steel) and needle valve (High speed steel, HSS), fitted together with very strict tolerances. The design of the nozzle, i.e., the number of orifices, their diameters, positions and drilling angles depend on specific engine application. The current trend is to use multi-hole nozzles with very small holes with diameter of only 0.10 - 0.14 mm in order to improve the fuel atomization and flow pattern.

Heat treatments are applied to the body and the needle to obtain the necessary hardness both on the surface and in the core of the parts and to face the following problems:

- fatigue failures at high stress areas due to repeated pulses of very high injection pressures;
- thermal shocks.

Adequate finishing of the orifice surfaces is very important also to optimize the erosion resistance.

The usage of new diesel blends characterized by different physical and chemical properties as compared with the traditional fuels could lead to modifications both in the choice of materials, geometry and positioning of orifices or their surface finishing to ensure the correct spray pattern. This work describes the results of our recent studies aimed at solving the problems related to the introduction of new eco-friendly oils and lubricants.

2. New prototype engine oils

2.1. Oil characterization

Three different synthetic ester base oils have been selected to formulate three prototype engine oils with the same additive composition. These oils are different mixtures of fully saturated polyglycol-ester and mono-ester types and designated as SEMO 4, SEMO 5 and SEMO 10. Same additive package has then been added to the three bases. After comparative characterization

of these prototype oils and selection of the oil with the best tribological performance (SEMO 10), a new improved formulation was developed based on the selected lubricating oil, designated SEMO 36. In addition, conventional mineral oil for two-stroke engines was used as reference oil. The additive package composition of the reference oil is different but it is ash-free as well as the other SEMO oils.

Oil viscosity was characterized according to ASTM D-445-06 standard procedure in [3], and viscosity index was determined using ASTM D-2270-04 in [4].

Deposit forming tendency of the oils was characterized by the Coker test at 250 °C during 12 h. Some physical and rheological properties of the lubricating oils are shown in Table 1. Among the prototype lubricating oils, SEMO 10 has the lowest viscosity both at 40 and 100 °C, the highest flash point and the lowest deposit forming tendency.

Unleaded petrol (E228) and bioethanol E85 (mixture of 85% of ethanol with 15% of gasoline) were selected to test miscibility of the lubricating oils with standard and alternative fuels. For this purpose two different lubricant/fuel ratios were used. Regarding to the miscibility method A (90% lubricant in fuel), SEMO 10 as well as SEMO 5 demonstrated good miscibility both with unleaded petrol and E85. Compared to this, the results for the 2% mixtures according (method B) differed. All tested lubricants proved to be perfectly miscible with EN228 fuel, whereas only SEMO 36 demonstrated to be fully miscible with E85. According to both miscibility methods the reference oil was only miscible with EN228. SEMO 36, when compared to its original prototype SEMO 10, has a much higher viscosity. Flash point for this lubricant is lower than for SEMO 10 but still higher than 200 °C.

		Ref. Oil	SEMO 4	SEMO 5	SEMO 10	SEMO 36
Density, g/ml	0.877	0.915	0.917	0.935	0.999	
Viscosity @ 40°C, mm ² /s	59.5	84.9	94	45.8	113.3	
Viscosity @ 100°C, mm ² /s	8.6	12.5	13.2	8.0	18.3	
Viscosity index	117	144	140	147	181	
Flash point, °C	120	204	190	260	218	
Pour Point, °C	-21	-39	-33	-39	not tested	
Deposit forming *	9	4	3	9	not tested	
Miscibility Method A (90% lubricant in fuel)	EN228	Good	Good	Good	Good	not tested
	E85	Poor	Poor	Good	Good	Good
Miscibility Method B (2% lubricant in fuel)	EN228	Good	Good	Good	Good	Good
	E85	Poor	Poor	Poor	Poor	Good

*Rating on base 10

Table 1. Properties of the engine oils

Wettability of the surface of the cylinder liner by lubricating oil is important for corrosion- and wear-protection of the piston rings and cylinder liner at the start-up when the temperature of the components is low. In this work, the wetting characteristic of the tested oils was determined using the Sessile Drop method. The resulting contact angles of the drops of various oils on the honed surface of the cylinder liner are shown in Table 2. Same method could not be used to determine wettability of the piston ring because of the small width of the ring. Therefore, the following procedure for qualitative comparison of the wettability of the piston ring by different oils in [12] was applied: 1 μ l of oil was placed on the circular flat surface of the phosphate cast iron piston ring and then, after 30 s, the extension of the oil drop along this surface was measured.

Oil	Contact angle on honed cast iron, ($^{\circ}$)	Spread distance of the oil on the piston ring, (mm)
SEMO 4	46.1 \pm 3.1	5.33 \pm 0.04
SEMO 5	43.4 \pm 0.2	5.39 \pm 0.05
SEMO 10	33.1 \pm 1.1	7.01 \pm 0.12
SEMO 36	50.8 \pm 0.5	3.78 \pm 0.17

Table 2. Contact angle and oil spread distance

The contact angle for SEMO 36 oil on the honed cast iron was the highest among all the tested lubricating oils. The contact angles of SEMO 5 and SEMO 4 were very similar one to each other and only slightly lower than for SEMO 36. SEMO 10 had the lowest contact angle and the largest drop spread for all tested oils. The behaviour of the drop spread of the tested lubricating oils over the piston ring surface is similar to that of the contact angle, bearing in mind that large contact angle values correspond to small spread distances.

Biodegradability and toxicity of the lubricating oils were examined according to the recommendations of the Organization for Economic Co-operation and Development (OECD) in [5]. Biodegradability of lubricating oils was tested using OECD 301F Manometric Respirometry Method consisting of the measurement of oxygen uptake by a stirred solution of the test substance in a mineral medium, inoculated with micro-organisms in [6]. Toxicity of the lubricating oils was studied using "Alga, Growth Inhibition Test" OECD 201 in [7] and "Daphnia Magna" 24 h Acute Immobilisation Test OECD 202 in [8]. In the "Alga, Growth Inhibition Test", selected green algae were exposed to various concentrations of the test oils over several generations under defined conditions. Results of biodegradability test are shown in Table 3. As expected, all synthetic ester base oils successfully passed the biodegradability test, while the reference mineral oil was not biodegradable according to the standard procedure OECD 301 Biodegradation of SEMO 5 and SEMO 10 exceeded 70%. In toxicity tests both with Alga and Daphnia Magna, the oils were classified as not harmful for aquatic organisms according to the standard procedures OECD 201 and 202 (see Table 4).

Time (days)	SEMO 4	SEMO 5	SEMO 10	REF
7	29.4	41.3	25.2	27.6
14	36.2	68.4	53.5	38.7
21	52.0	79.6	69.6	33.4
28	61.1	81.2	75.7	51.2
Ultimate	> 60%	> 60%	> 60%	< 60%

Table 3. Biodegradability of oils (% of biodegraded oil) in [12].

Oil	EC50/EL50 with Alga, mg/l	Classification OECD 201	EC50/EL50 with Daphnia Magna, mg/l	Classification OECD 202
SEMO 4	>100	not harmful *	>1000	not harmful *
SEMO 5	>100	not harmful *	>1000	not harmful *
SEMO 10	>100	not harmful *	>1000	not harmful *
SEMO 36	-	-	>1000	not harmful *

*With respect to aquatic organisms.

EC50/EL50 is that concentration of test substance which results in a 50% reduction in either growth or growth rate relative to the control.

Table 4. Results of the toxicity tests in [12].

2.2. Tribological evaluation according to DIN 51834-2

Tribological evaluation of lubricating oils was done using ball-on-disk configuration with reciprocating motion according to the standard procedure DIN 51834-2 in [9]. Ball and disk were made of 100Cr6 steel. The ball, 10 mm in diameter, performed reciprocating motion with a stroke of 1 mm and a friction frequency 50 Hz. Normal load was 50 N during short run-in period 45 s and 300 N during the test 60 min. The ball and the disk were immersed in the lubricating oil, which temperature during the test was constant and 50 °C. Friction force was measured as function of time. Friction coefficient was calculated as the ratio of the tangential force to the normal force.

After test completion, diameter of the wear scar on the ball was measured using optical microscope, and, from this data, volume wear of the ball was calculated for each lubricating oils tested.

Evolution of the friction coefficient in friction evaluation tests is shown in Figure 1. Oils with low additive content: SEMO 4, SEMO 5 and SEMO 10 showed an interval of frictional instability after the run-in period. In the instability period, which lasted from 400 up to 800 s, there are some sharp peaks indicating damage of surface and seizure, probably due to micro-welding. The reference lubricating oil had a less pronounced instability period without sharp

peaks, while SEMO 36 did not present any instability. Final values of friction coefficient after 60 min and the diameters of the wear scar on the ball are shown in Table 5.

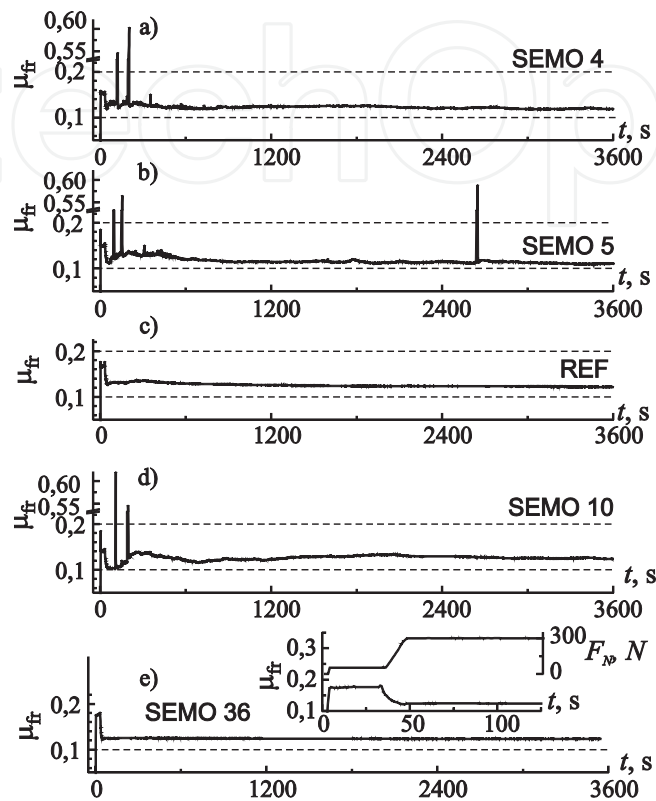


Figure 1. Evolution of friction coefficient in time during tribological evaluation tests of the following oils: a) SEMO 4, b) SEMO 5, c) reference oil, d) SEMO 10, e) SEMO 36. Inset in graph e) shows the initial part of the plot together with the curve of the normal load in [12].

Oil	Final μ_{fr}	Diameter of wear scar, μm	Estimation of worn volume, mm^3
SEMO 4	$0.119 \pm 3.40 \cdot 10^{-5}$	884	$6.01 \cdot 10^{-3}$
SEMO 5	$0.111 \pm 4.34 \cdot 10^{-5}$	885	$6.02 \cdot 10^{-3}$
REF	$0.122 \pm 2.73 \cdot 10^{-5}$	517	$6.99 \cdot 10^{-4}$
SEMO 10	$0.125 \pm 3.81 \cdot 10^{-5}$	929	$7.32 \cdot 10^{-3}$
SEMO 36	$0.123 \pm 1.54 \cdot 10^{-5}$	459	$4.36 \cdot 10^{-4}$

Table 5. Friction coefficient and wear of the ball in tribological evaluation test of oils (DIN 51834-2) in [12].

The volume of worn material of the ball was estimated geometrically on the basis of the diameter of the wear scar using the following equation (1):

$$V = \frac{\pi}{3} (R^3 - (R^2 + a^2)\sqrt{R^2 - a^2}) \quad (1)$$

where $R = 5 \text{ mm}$ is the radius of the ball and a is the radius of the circular wear scar.

Wear specific energy, E_w , that is, the ratio of the dissipated energy, E , during friction per unit mass of worn material Δm , is an important characteristic which shows the ability of a material to resist wearing. This is a complex parameter taking into account both friction, which characterizes energy supply to the material in the friction zone, and wear intensity. This parameter is considered a very useful tool to compare standard tribological evaluation and simulated tests in [10]. Wear specific energy was determined using the following equation in [12]:

$$E_w = \frac{E}{\Delta m} = \frac{v_m F_N \int_{t_i}^{t_f} \mu_{fr}(t) dt}{\Delta m} \quad (2)$$

Where v_m is mean sliding velocity obtained with a reciprocating frequency of 50 Hz and 1 mm stroke, F_N is the normal load, μ_{fr} is the friction coefficient, t_i and t_f are respectively the initial and final time points of friction test time interval.

In this study, only ball wear was determined as specified by DIN 51834-2. So, the absolute value of wear specific energy could not be determined; since wear of the disk was not measured. However, by using the ball mass loss in the denominator of eq. (2), the upper bound estimation of the wear specific energy can be determined. This upper bound can be used for qualitative comparison of anti-wear properties of the lubricating oils under constant friction conditions. These values, determined using eq. (2), are shown in Figure 2. SEMO 36 and the reference oil have much higher values of the wear specific energy, than other oils. Therefore, these lubricating oils improve contacting surfaces wear protection since much larger energy should be dissipated to produce the same wear as compared to SEMO 4, SEMO 5 and SEMO 10 lubricants.

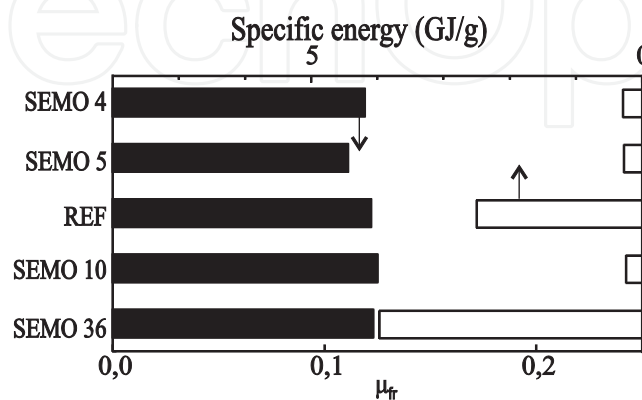
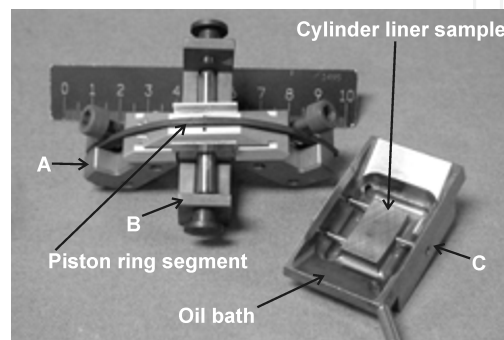


Figure 2. Friction coefficient and wear specific energy in [12].

2.3. Piston ring/cylinder liner simulation

Tribological simulation was performed using cast iron phosphated piston ring and cast iron cylinder liner using reciprocating motion configuration. The samples for the tests were cut from real engine parts (Minsel M165 two-stroke engine manufactured by Abamotor Energía) keeping original curved surfaces and surface finishing. The conformal contact between the piston ring and the cylinder counterpart was reproduced by placing a piston ring on a suitable frame, A, and fixing it by means of a clamp, B (Figure 3). Wear of the components was determined by weighting and geometry measurements.



A - frame for fixing the piston ring segment, B - fixing clamp, C - base with oil bath for fixing cylinder liner sample.

Figure 3. Experimental set-up for piston ring/cylinder liner simulation.

The piston ring segments performed a reciprocating motion with a stroke of 1 mm and a friction frequency 40 Hz. Normal load was 50 N during short run-in period 45 s and 300 N during the test 90 min. During the test, the piston ring segment and the cylinder liner sample were immersed in the oil, which temperature was constant at 200 °C.

The mass change of the piston ring segments and cylinder liner sample was determined from weighting the components before and after friction tests. Since the mass change can be due to two competitive processes: (i) wear out and (ii) deposit formation from the oil at elevated temperature, estimation of wear out by weighting can give erroneous results. Indeed, after the tests the surface colour became yellowish and remained after dissolvent cleaning indicating some sparingly soluble deposits formed on the surface due to some chemical reaction. Therefore, in addition to the determination of the mass change, worn volume was calculated from surface geometry. Surface morphology of the friction zone was studied using white light confocal microscopy at three different zones along the wear track on the cylinder liner sample. The acquired 3D surface images were 0.5 mm wide in the direction of friction and each image contained 138 cross-section profiles of the wear track yielding totally 414 profiles for each sample. Firstly, the cross-section profiles were averaged for each sample and then among different samples tested using the same lubricating oil. Worn volume of the samples of cylinder liner was calculated as a product of a mean cross-section area of the groove and the total length of the groove. The cross-section area was determined by numerical integration of the cross-section profiles and then worn mass was calculated from the worn volume using the density of cast iron.

Surface chemical composition of the friction zone of cylinder liner samples was characterized using Energy Dispersion X-Ray Spectroscopy (EDS).

Evolution of friction coefficient in time during friction between piston ring segment and a piece of the cylinder liner is shown in Figure 4. It is possible to highlight the increment of the coefficient of friction μ_{fr} for lubricants SEMO 4 and SEMO 5 overtaking the constant value reached by the lubricant of reference. In fact, for SEMO 4 and SEMO 5, friction coefficient gradually rose during the experiment (90 min) and did not stabilize. The growth behaviour was almost linear in time.

Initial friction coefficient was about 0.2 and the final one about 0.33 in both cases. SEMO 10 and SEMO 36 showed different behaviour. The initial values were 0.2 and 0.14 for SEMO 10 and SEMO 36, correspondingly.

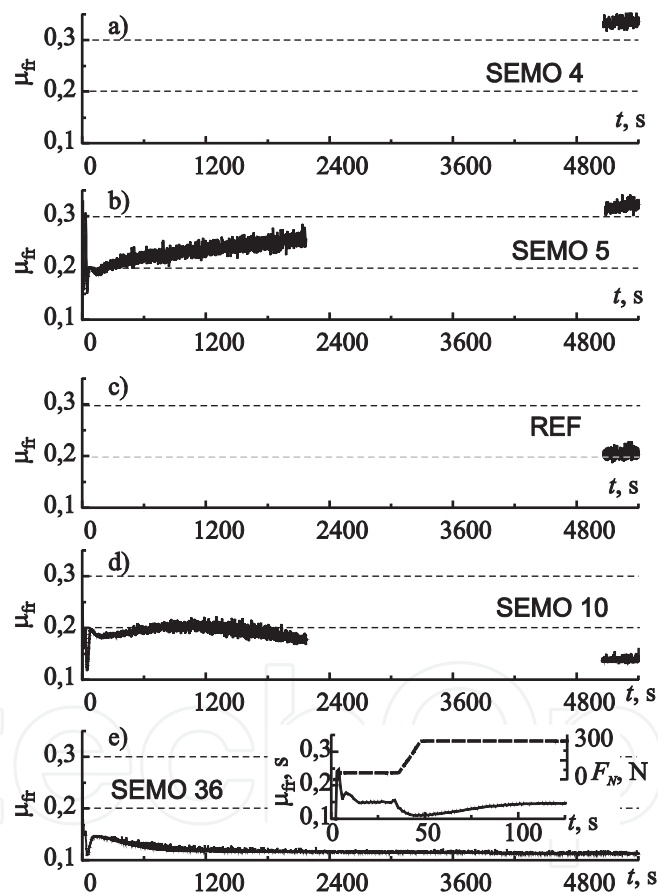


Figure 4. Evolution of friction coefficient in time during piston ring/cylinder liner simulation test. a) SEMO 4, b) SEMO 5, c) reference oil, d) SEMO 10, e) SEMO 36. Inset in the graph e) shows the initial part of the plot together with the curve of the normal load in [12].

At the beginning, after a run-in period, friction coefficient increased and reached maximum. For SEMO 36 the maximum was reached usually between 100 and 200 s from the beginning of the test, while for SEMO 10 the period of increase was longer and the maximum was reached

after 700 to 1700 s from the beginning of the test. After reaching the maximum, friction coefficient decreased slowly and stabilized at 0.14 and 0.11 for SEMO 10 and SEMO 36, correspondingly. The friction coefficient of lubricant SEMO 10 showed a slow decline until reaching a constant value lower than the reference one. Friction coefficient for the improved lubricant SEMO 36 levelled out rapidly at a very low value and showed less scatter, probably due to some sort of surface deposition on the contact surfaces.

The averaged cross-section profiles of each liner sample tested are reported in Figure 5. Different scales of magnitude are used for better visualization of the mean contact surface profile. It is possible to notice very good performance of the lubricant SEMO 10 and its improvement in the lubricant SEMO 36. Samples tested using SEMO 4 and SEMO 5 had deep grooves with the maximum depth 22 to 25 μm . The samples tested using the reference oil and SEMO 10 had less deep grooves with a maximum depth of 4 to 5 μm . Surface of the samples tested using SEMO 36 oil had some thin scratches in the direction of friction while grooves had not been formed.

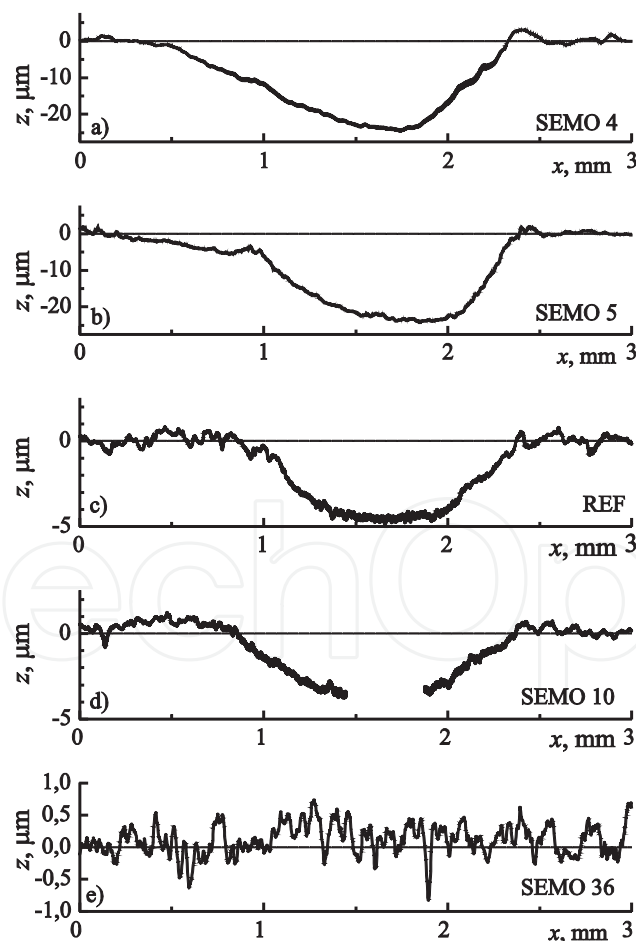


Figure 5. Average cross-section profile of the friction zone of cylinder liner samples tested using different lubricants in [12].

Figure 6 shows images of the friction zone of the piston ring segments after friction simulation tests with different lubricating oils. Wear and damage of the surface as function of the oil used was similar to that in the cylinder liner. In tests with SEMO 4 and SEMO 5, the material in the friction zone was heavily damaged. The wear can be classified to be of the adhesive type with intensive plastic deformation and edging. When the reference oil and SEMO 10 oil were used in the tests, the damage of the material was less pronounced than for SEMO 4 and SEMO 5, but the wear in all cases was of the adhesive type. Only small damage was observed on the piston ring segments when using SEMO 36. In this case, only summits of the circular grooves of the piston ring presented some wear and deformation. From the point of view of hydrodynamic lubrication these results may seem to be surprising, since, with the same additive composition, higher wear rate occurs for thinner oil (SEMO 10 in our case) than more viscous oils (SEMO 4 and SEMO 5). Therefore, these results lead to the following conclusions: 1) the lubrication regime should be of a boundary type and 2) surface protection against wear for SEMO 10 and SEMO 36 oils seems to be resulting from the formation of surface layer as a result of adsorption of oil components or tribochemical reactions between the oil components and the base material.

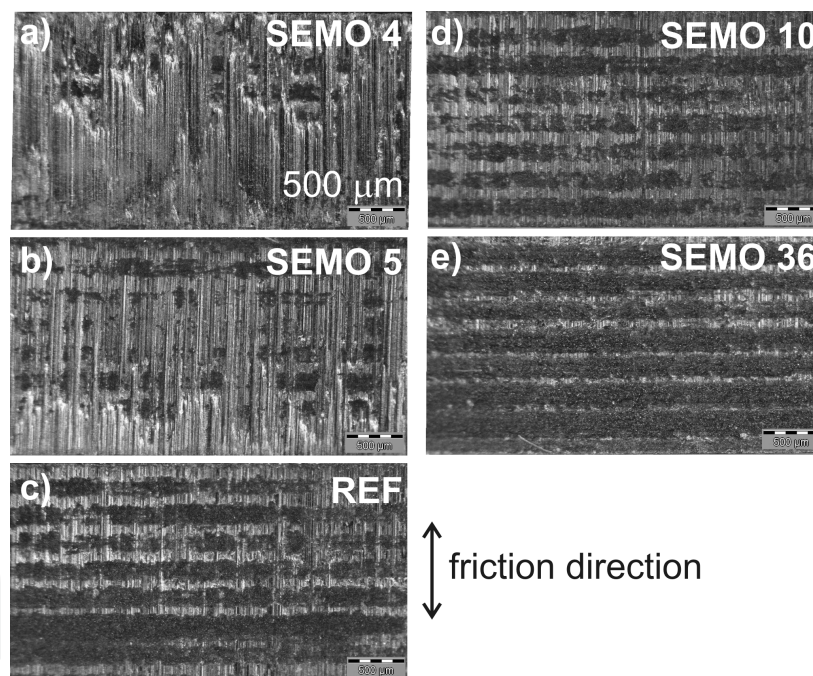


Figure 6. Optical images of the friction zone of the piston ring segments after friction simulation tests using different lubricants. The scale of each image is the same and shown by a scale bar in [12].

Results of the mass change measurements of the components are shown in Table 6. Worn mass calculated from the worn volume is plotted vs. measured mass change in Figure 7 (dots). The experimental data are fitted by linear function with two adjusted parameters: slope and intersect (dashed line in Figure 7). The solid line is a linear fit with a fixed slope 1 and adjusted intersect. Coefficients of determination for these linear regressions are 0.983 and 0.949, correspondingly, indicating statistically significant linear relationship between the mass

change and worn mass determined from the geometry of the groove. Therefore, the deposit formation has not much influence on the mass change and the last can be used as a measure of the components wear out in these tests. The upper bound of the wear specific energy was determined in accordance with eq. (2), using the cylinder liner mass change in the denominator of eq. (2).

Oil	Final μ_{fr}	Mass change, mg		Worn volume (cylinder.) mm ³
		cylinder	segment	
SEMO 4	0.34	-3.95	-1.41	$-1.12 \cdot 10^{-2}$
SEMO 5	0.32	-3.68	-3.22	$-9.8 \cdot 10^{-3}$
REF	0.20	-1.1	-0.64	$-1.74 \cdot 10^{-3}$
SEMO 10	0.14	-0.94	-1.25	$-2.3 \cdot 10^{-3}$
SEMO 36	0.11	-0.09	1.23	0

Table 6. Results of friction simulation tests in [12].

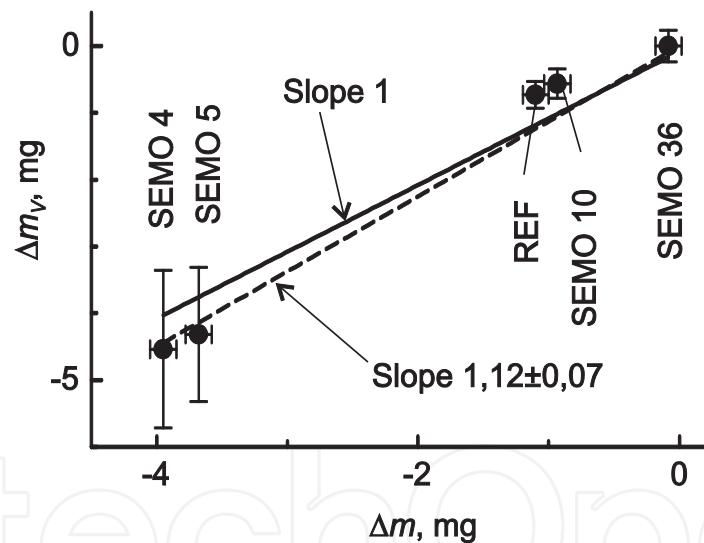


Figure 7. Mass wear determined from the geometry of the groove vs. mass change of the cylinder liner samples. The dashed line is a linear regression of experimental data with two adjusted parameters: slope and intercept. The solid line is a linear regression with a fixed slope 1 in [12].

Final friction coefficient and wear specific energy are shown in Figure 8. SEMO 36 oil showed the best antifriction and wear resistance characteristics among all tested lubricants. Friction coefficient was almost a half of that for the reference oil, while specific wear energy was 7.8 times higher than for the reference oil. In comparison with the ball-on-disk tests, wear specific energy for SEMO 36 lubricant was much lower in the tribological simulation test; however, oil temperature in these two tests was different. When the ball-on-disk evaluation tests were performed at the same temperature as in the simulation test (200 °C), the value of wear specific

energy was similar to that in the simulation test: 0.14 GJ/g in the ball-on-disk at 200 °C vs. 0.18 GJ/g in the piston ring/cylinder liner simulation test. Although these values are only upper bound estimations of the real values, they are close to one another. According to the structural-energetic approach in [10], this means that the dominating wear mechanism in both cases is the same. Then, a significant decrease in the wear specific energy from 3.97 to 0.14 GJ/g with temperature increase from 50 to 200 °C implies changing in dominating wear mechanism at higher temperature. It can be stated that, under the applied experimental conditions, the chemical compositions of the base oil and the additives had greater influence on the tribological performance of the lubricants than their rheological properties.

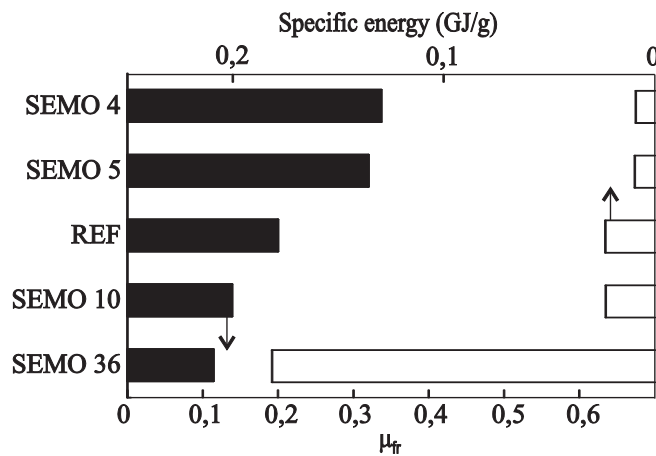


Figure 8. Friction coefficient and wear specific energy in friction simulation tests in [12].

2.4. Surface characterization

Surface chemical composition of the friction zone of cylinder liner samples was characterized using Energy Dispersive X-Ray Spectroscopy (EDS). Table 7 shows surface chemical composition for three different surfaces:

- friction zone of the cylinder tested using SEMO 36 lubricant,
- untouched surface of the same cylinder, and
- reference cylinder not immersed neither heated in lubricating oil.

	Fe	O	C	Si	Mn
Friction zone	61.5±1.9	11.5±0.7	23.5±3.2	2.83±0.68	0.615±0.085
Untouched zone	84.0±3.6	7.36±0.46	3.41±3.31	4.19±0.07	1.11±0.17
Reference sample	92.5±0.3	2.95±0.46	0.1	3.59±0.52	0.935±0.255

Table 7. Surface chemical composition (at.%) of the cylinder liner samples tested with SEMO 36 lubricating oil

Silicon and manganese were alloying elements of the base material and did not show important variations in their concentration, whereas the most important variation was in the carbon and oxygen content. There was no significant difference for other elements since the oils had no metal-containing additives. Figure 9 shows surface concentration of four elements relative to iron. After the test, during which a cylinder was immersed in the SEMO 36 oil and heated at 200 °C, carbon and oxygen concentrations on untouched surfaces were slightly higher than on the reference sample, e.g., the sample not immersed into the oil. However, carbon and oxygen concentrations drastically increased on the surface of the friction zone, on which carbon was each forth atom. Also, in contrast to the untouched surface and the reference surface, on the surface of the friction zone, carbon concentration was higher, than the oxygen one. One can infer from these data that friction induced tribochemical reactions between oil components and base material to form surface layer enriched with carbon and oxygen. This surface layer or sliding lacquer may protect mating surfaces from adhesion and/or damage yielding lower friction and wear in [10].

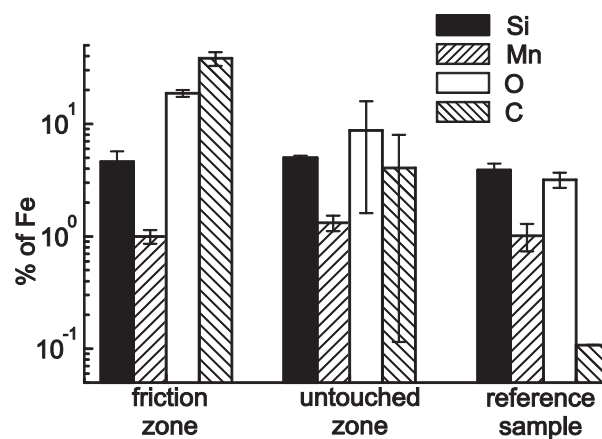


Figure 9. Surface concentration of elements relative to iron in [12].

2.5. Experimental evaluation in real two-stroke engines (Minsel M165)

After previous simulation tribological test the performance of the oils was evaluated in real two-stroke engines (Minsel M165) with a swept volume of 158 cm³, a stroke of 54 mm, compression ratio 7,1:1, power (ISO 1585) 3.53/4.8 kW/HP, maximum torque 120 Nm and 4500 rpm rotation speed. Scuffing tests were performed using various lubricating oil – petrol mixtures in order to evaluate the lubricating performance of the lubricants under extreme load conditions. The test conditions applied are shown in Table 8, and the tested oil-fuel compositions are shown in Table 9.

Figure 10 shows the photographs of the engine components after scuffing tests, in which the reference mineral oil was used in a mixture with pure petrol and bioethanol. Increase in the bioethanol content in the fuel led to decrease in carbon soot deposition on the engine cylinder and piston. Also, when bioethanol was used, the surface was less damaged under extreme working conditions.

Test step	Speed, rpm	Time, min	Power	
			%	HP
1	2000	5	0	0
2	4000	20	50	2.4
3	4000	20	75	3.2
4	2000	5	0	0
5	4500	90	100	full load
6	2000	5	0	0

Table 8. Experimental conditions for scuffing tests of real two-stroke engines

Fuel	Reference oil	New developed oils	
		SEMO 10	SEMO 36
Petrol	2%	2%	2%
E10	2%	-	-
E20	2%	-	-
E85	2%	-	2%

Table 9. Oil – petrol combinations tested in a real two-stroke engine scuffing test

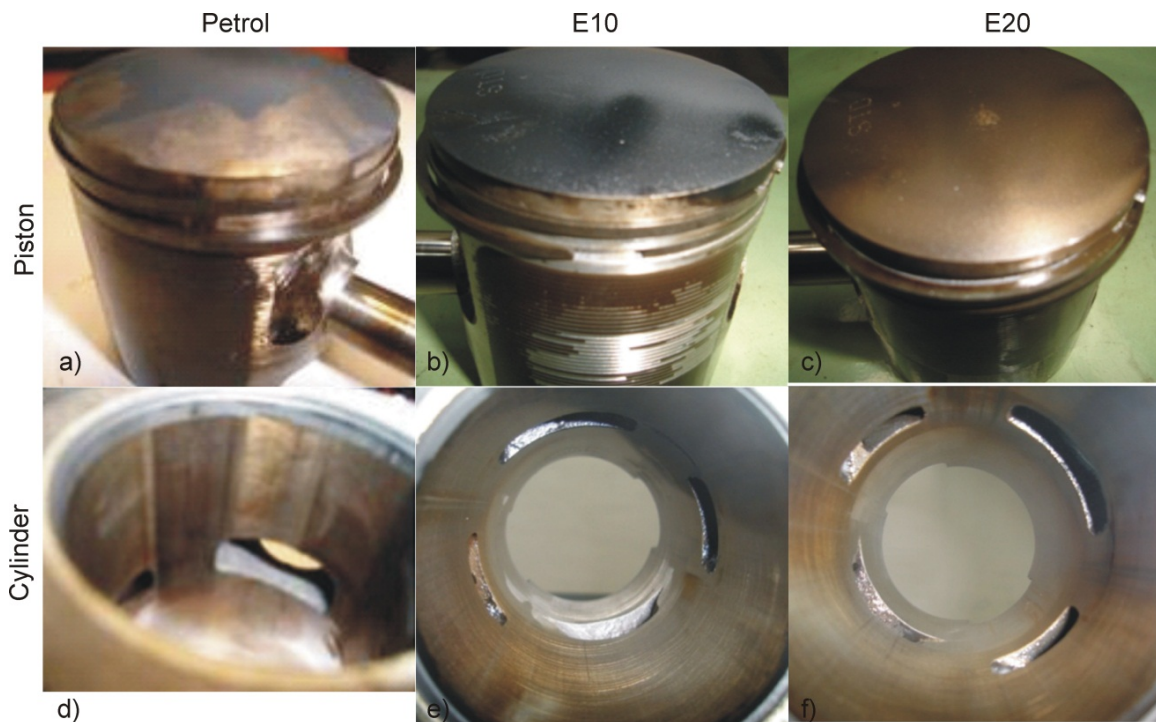


Figure 10. Macro images of two-stroke engine components after scuffing test using a mixture of mineral oil with petrol (a,d), bioethanol E10 (b,e) and bioethanol E20 (c,f) in [12].

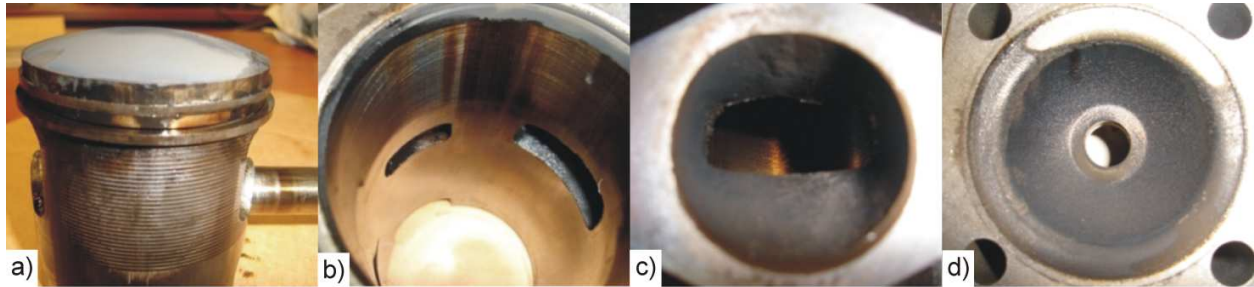


Figure 11. Macro images of two-stroke engine components after scuffing test using mixture of SEMO 10 lubricating oil with petrol: a) piston, b) cylinder, c) exhaust side, d) intake in [12].

Figures 11 show the photographs of the engine components after scuffing tests using a SEMO 10 – petrol mixture. Some seizure between compression piston ring and cylinder was observed when using a mixture of SEMO 10 with petrol. Several vertical abrasion marks were formed in the exhaust zone of the cylinder, where the temperature was higher. However, the piston and cylinder were quite clean with only some carbon soot deposits in the exhaust zone. The state of the cylinder head was quite healthy and clean in the intake zone, the carbon residues were considered normal.

Figure 12 shows the pictures of the engine components after scuffing test using SEMO 36 lubricating oil with petrol and bioethanol fuels. When using a mixture of SEMO 36 with bioethanol E85 or petrol, no scuffing or seizure was observed. Only light scratches were found on the cylinder surface, which were more pronounced when using petrol. In this case, carbon soot deposits formed intensively on the top part of the piston. The piston and cylinder were very clean, when using bioethanol.

In addition, gaseous emissions from the engine were analyzed for various fuel-oil mixtures with different proportions of bioethanol to petrol: 20%, 30% and 85%. The gas emissions were measured using the Directive CE 2002/88, Portable, SH3 modality as reference limits. The differences in power and consumption were negligible when using bioethanol E10 and E20. When compared with the petrol, the NO_x emissions showed an increasing trend and the emissions of CO and CH diminished in tests with bioethanol and reference oil. When using E85, the reference mineral oil was not miscible, but the new developed oil SEMO 36 was totally miscible. When using bioethanol E85, a considerable reduction in engine power was observed yielding value 13% to 22% less than in the tests with petrol. At the same time fuel consumption increased slightly between 7% and 20%, and gaseous emissions were considerably reduced (see Table 10). When using SEMO 36 the reduction in NO_x emission was the most significant as compared with other gases and was probably due to the lower temperature generated.



Figure 12. Macro images of two-stroke engine components after scuffing test using mixture of SEMO 36 lubricating oil with bioethanol E85 (a, b, c) and petrol (d, e, f): a), b), d), e) piston, c), f) cylinder in [12].

Oil Type and %	Power (kW)	Consumption (g/kWh)	NO _x (g/kWh)	CH _x (g/kWh)	CO (g/kWh)
SH3 Limit Normative			5.36	161	603
Petrol/Ref. Oil 2%	5.46	397	1.469	139.8	333.2
E10 + 2% Ref. oil	5.44	385	1.573	124.1	314.8
E20 + 2% Ref. oil	5.5	382	2.29	128	251.5
E85 + 2% Ref. oil (not miscible)	4.8	427	2.29	109.8	43.11
E85 + 2% SEMO 36 (miscible)	4.3	478	0.689	119.5	32.93

Table 10. Emission of gases from two-stroke engine tested with different lubricating oil– petrol combinations in [12].

2.6. Life cycle

The lifecycle analysis for a 2-stroke engine fed by petrol and E85 was carried out using the model M 165 Minsel engine running in a tiller during 1000 h, which characteristics are shown in Table 11.

Model of machine	Tiller 3002
Machine weight	90-110 kg
Engine model	M165 Minsel 2-stroke
Engine weight	12.8 kg
Engine life	1000 h
Scuffing test results	OK
Engine power	3 kW
Emissions	Directive 97/68/CE and later 2002/88/CE and 2004/26/CE

Table 11. Characteristics of the engine used in life-cycle analysis

Two fuel + oil pairs named as “Cleanengine systems” were compared with the Conventional system for the same engine working in the same application. In the alternative Cleanengine system I the engine was fed by a mixture of bioethanol E20 and mineral oil. In the alternative Cleanengine system II, the engine was fed by bioethanol and newly developed advanced and biodegradable lubricating oil SEMO 36. The fuel and oil consumption for the conventional and two alternative systems is shown in Table 12.

	Conventional	Cleanengine system (I)	Cleanengine system (II)
Fuel consumption per functional unit	Petrol 900 kg	BioE20 1123 kg	BioE85 1405 kg
Oil consumption per functional unit	Mineral oil 36 kg	Mineral oil 23 kg	SEMO 36 29 kg

Table 12. Parameters of the conventional and alternative systems used in the life-cycle analysis

The Eco-indicator 99 Methodology was used for the Impact Assessment method. The components of the environmental impact are shown in Figure 13 a), while the total environmental impact is shown in Figure 13 b). Almost all components of the environmental impact as well as the total environmental impact were higher for fossil fuel. However, the climate change was more affected by the renewable system.

The global environmental impact evaluated by Lifecycle Assessment tools for the Cleanengine system I and II using bioethanol was lower than for the reference system using petrol. The comparison between two alternative systems Cleanengine I and Cleanengine II showed that the last one had slightly higher environmental impact due to higher fuel and lubricant consumption that can be related to the lower calorific value of the ethanol compared to the petrol. While the reduction of the environmental impact is attributed to the reduction in emissions, the use of a biodegradable nontoxic lubricant will further reduce the environmental impact of the Cleanengine II system.

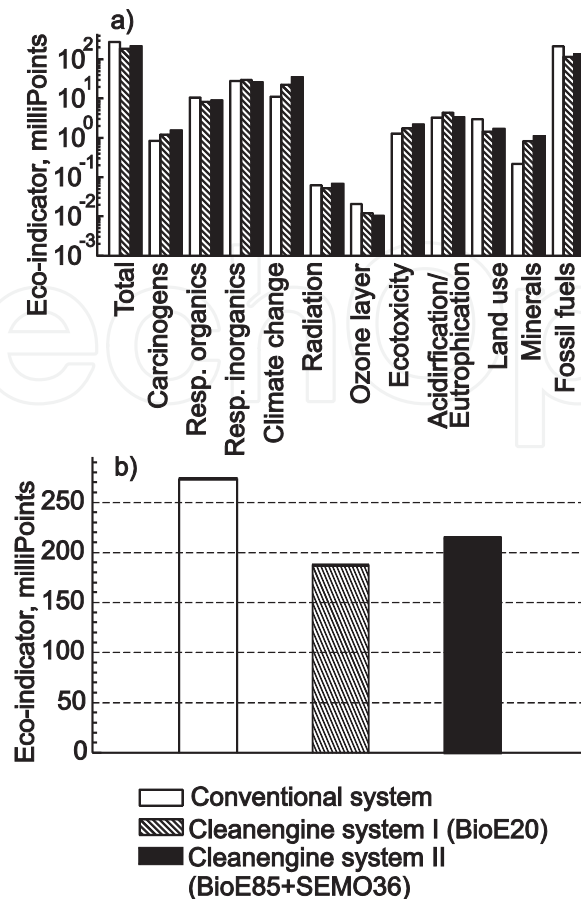


Figure 13. Results of the life-cycle and environmental impact analysis for the conventional and two alternative systems: a) components of the environment impact, b) total environmental impact in [12].

3. Nozzles for future engines

Compared to conventional liquid hydrocarbon fuels, bio-fuels exhibit considerable differences in their physical properties which significantly influence on the injector flow as well as on primary and secondary spray break-up processes. As a consequence, spray mixture formation of bio-fuels is considered to be largely different compared to conventional fuels under engine operating conditions with severe consequences on the combustion and emission characteristics. Hence, injection and combustion system optimization as well as optimization of the injector configuration (number of nozzle holes, diameter, spray targeting, etc.) for bio-fuels requires a detailed knowledge of how the fuel properties influence the injector flow and spray atomization characteristics. Optimization of the nozzles materials and design is an important task which will open new markets and enlarge the number of potential customers for eco-friendly applications.

3.1. Tribological evaluation

Different metal-doped DLC coatings were developed by Physical Vapour Deposition method (PVD). Friction and wear tests were carried out using SRV tribometer with "cylinder-on-disc" configuration in lubricated conditions. The coatings were deposited on steel cylinders and

disks. The cylinder, 15 mm in diameter, performed reciprocating motion with a stroke of 2 mm and a friction frequency 50 Hz. Normal load was 50 N during short run-in period 30 s and 200 N during the test 60 min. The cylinder and the disk were immersed in fluids, which temperature during the test was constant and 25 °C.

Both Cr- and Ti DLC coatings had good friction and wear behaviour and they could be a good alternative to improve tribological properties of the actual uncoated nozzles.

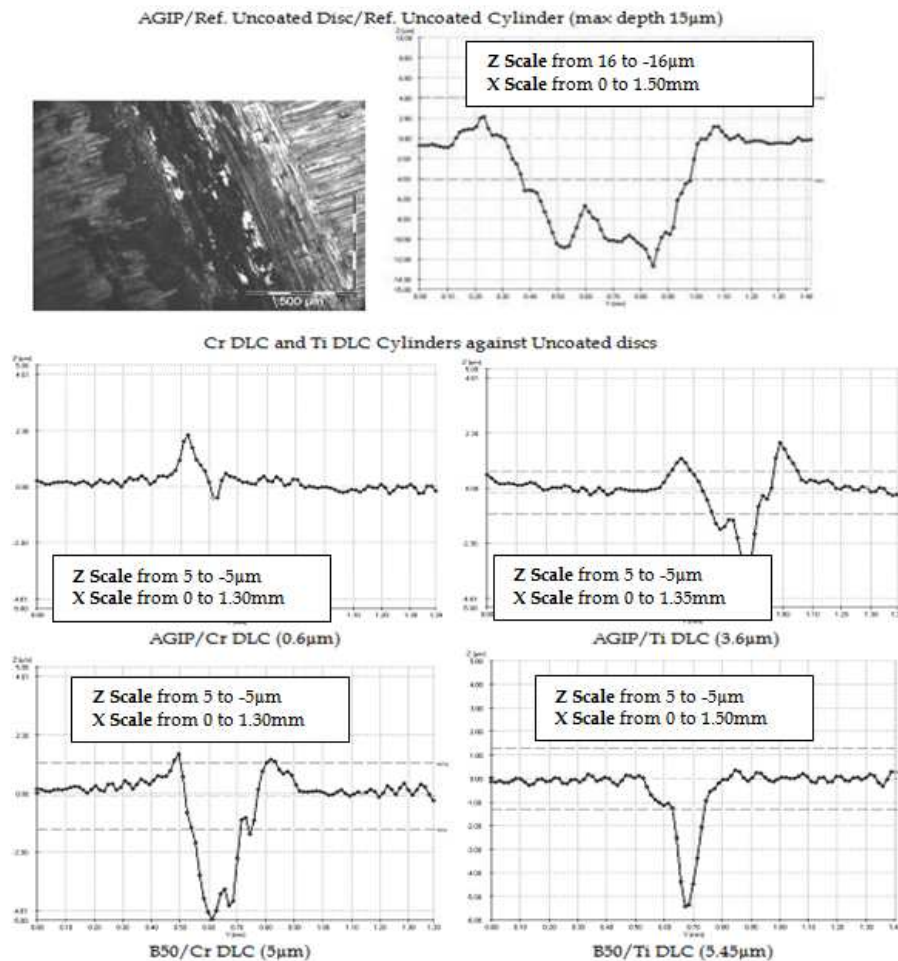


Figure 14. Average cross-section profile of the friction zone of discs samples (uncoated reference, Cr and Ti DLC) tested using different fuels, AGIP and B50. Different scales of magnitude are used for better visualization of the mean contact surface profile.

Surface morphology of the friction zone was studied using white light confocal microscopy. The averaged cross-section profiles for each sample tested are shown in Figure 14. It is possible to notice very good performance of the coatings, they had deeper grooves with a maximum depth of 5.45 µm. Cr DLC tested against AGIP fuel had better performance than Ti DLC. Two different scales of magnitude, Z, are used for better visualization of the mean contact surface profile. From 5 to -5 µm for coated discs (Cr DLC and Ti DLC lubricated with AGIP ref and B50) and from 16 to -16 µm for uncoated ref samples.

3.2. Corrosion characterization

Corrosion resistance of different materials and coatings used for nozzles fabrication (Cr and Ti DLC) was characterized using electrochemical impedance spectroscopy and potentiodynamic polarization techniques in order to determine the kinetics parameters and the corrosion mechanisms of these materials in NaCl 0.5M or K₂SO₄ 0.2M in [12].

Base nozzles material, uncoated steel X82WMo, was also characterized under corrosion conditions and compared with DLC coated samples of the same material. The electrolyte used in these tests was K₂SO₄ 0.2M. Cr DLC coating offered excellent corrosion protection. The coating did not exhibit any pores or defects, protecting effectively the substrate during immersion.

Open-circuit potential (OCP) was measured during 2200 s in order to analyze the samples tendency with the exposure time. After that, an electrochemical impedance spectroscopy was performed in a frequencies range from 10 k to 10 mHz. Once impedance measurements finished, a potentiodynamic potential swept was applied from OCP-0.2 V to OCP+0.6 V at a scan rate of 0.5 mV/s.

Coated nozzles had more positive potential than the reference ones. For all surfaces, OCP was stable after first 2200 s of immersion. The difference between three nozzles regarding impedance results was very notable. Cr and Ti DLC coated samples had a semicircle Nyquist diagrams implying that the electrolyte did not reach the substrate during the immersion in the dissolution. The coating acted as an effective protective barrier. Uncoated nozzle had lower corrosion resistance. Two time constants could be clearly distinguished from two maxima in the Nyquist plots.

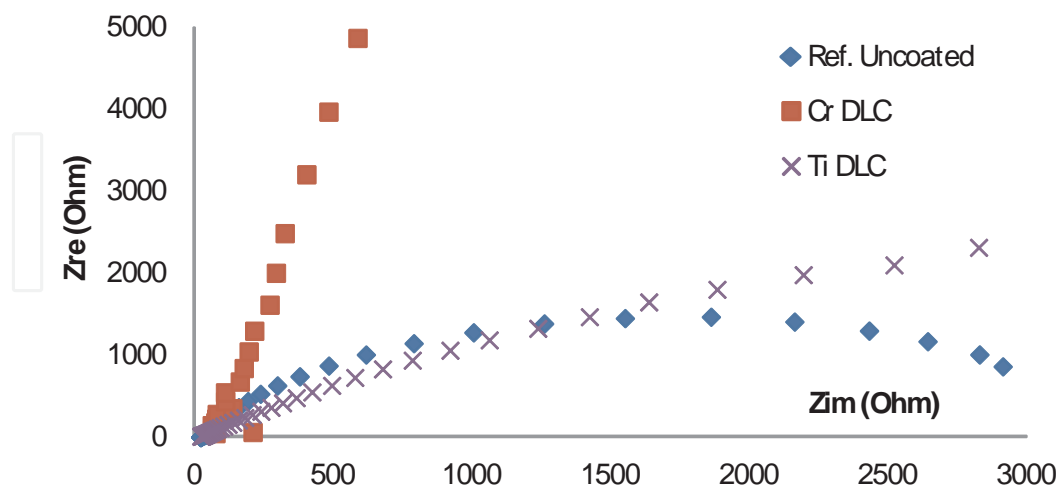


Figure 15. Nyquist diagrams. Impedance data of coated and uncoated nozzle in K₂SO₄.

Table 13 shows the parameters obtained from equivalent circuit simulation of the experimental data and Figure 16 shows the equivalent circuits used in the simulation process.

Samples (Nozzle appl.)	OCP (V)	R1 (k Ω /cm ²)	CPE1 (μ F/cm ²)	R2 (k Ω /cm ²)	CPE2 (μ F/cm ²)	ZO ($\mu\Omega$ -1- σ 1/2; σ 1/2)
Nozzle Uncoated	-0.556	0.035	$Y_o=58.45$ $n=0.82$	1.10	$Y_o=140.7$ $n=0.94$	
Nozzle Cr DLC	-0.022	12780	$Y_o=0.75$ $n=0.94$	-	-	-
Nozzle Ti-DLC	-0.354	10.38	$Y_o=0.34$ $n=0.639$	-	-	$Y_o=0.02$ $B=3.23$

Table 13. Equivalent circuit parameters of coated and uncoated nozzles

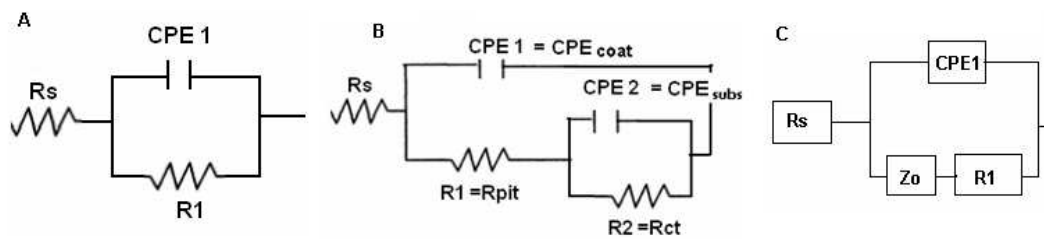


Figure 16. Equivalent circuits used for the experimental data simulation. Circuit A) for Nozzle Cr DLC; circuit B) for uncoated nozzle and circuit C) for Ti DLC coating.

Polarization curves for the coated nozzle are shown in Figure 17.

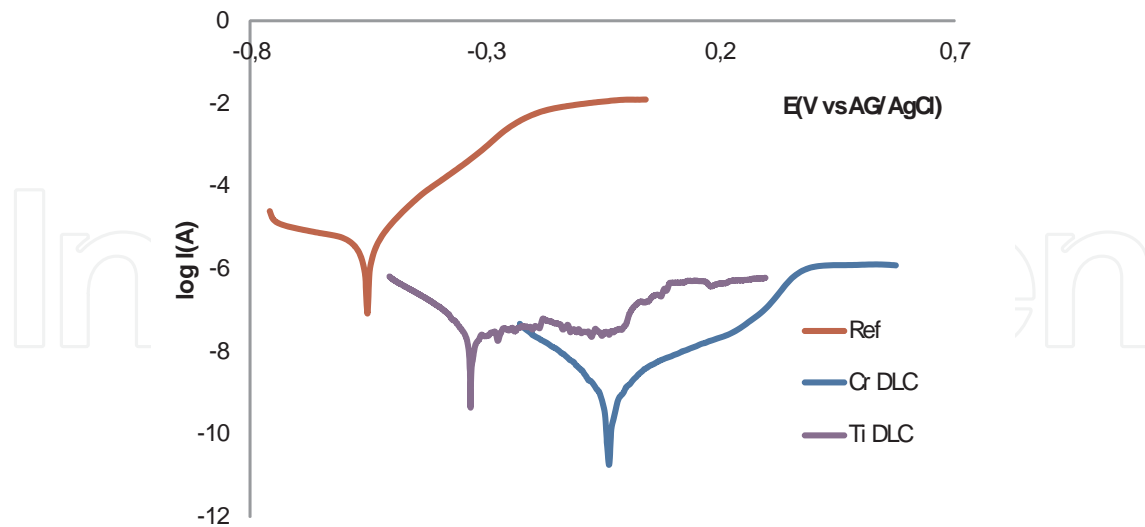


Figure 17. Polarization curves on coated and uncoated nozzles immersed in K_2SO_4

Cr DLC coating had passive behaviour and low corrosion current of the order of 10^{-9} A for potentials near to OCP. Coating Ti DLC also had passive behaviour in a wide zone of the anodic

branch. Cr DLC and Ti DLC notably improved substrate corrosion behaviour reducing its corrosion current by several orders of magnitude (see table 14).

Samples	E_{corr} (V)	I_{corr} ($\mu\text{A}/\text{cm}^2$)
Nozzle Ref. Uncoated	-0.533	18.5
Nozzle Cr DLC	-0.039	0.003
Nozzle Ti DLC	-0.331	0.18

Table 14. Corrosion current of coated and uncoated nozzles calculated using Tafel approach

3.3. Experimental evaluation in real four-stroke engines (Minsel M430)

The injectors were tested in the Minsel M-430 engine manufactured by Abamotor Energía, SL. The parameters of the engine and test conditions are shown in Table 15.

Bore	85 mm
Stroke	75 mm
Displacement	426 c.c.
Compression ratio	19,3: 1
Power NB	8,4 / 8,7 Cv
Rpm	3000
Torque	23Nm / 2000 RPM
Dry weight	45 Kg

Table 15. Characteristics of the engine used in engine tests to evaluate the different alternative nozzles (Cr DLC and Ti DLC).

During the test the engine worked for 50 hours at full load (3000 rpm). Biodiesel B30 was used as a fuel, which was a mixture of FAME (100% Biodiesel) with diesel B at a rate of 30%.



Figure 18. The engine on test bench and the tested nozzles installed on the engine

3.4. Nozzle characterization after test in the engine

Scanning electron microscope (SEM) and energy dispersion X-Ray spectroscopy (EDS) were used for characterization of the nozzles geometry after the engine tests. Cr DLC coating had better behaviour than Ti DLC.

The microanalysis showed that for the all coatings the deposited layer on the needle persisted after the test, with the exception of the tip where the Ti DLC layer has been detached

Additionally, the spray holes geometries of the nozzle body were analysed after endurance test with two different fluids: reference standard fuel and 30% biodiesel.

Figure 19 shows the scanning electron microscope images (EDS) of the nozzle body tip before the engine test (real part and its corresponding silicon model for orifices internal characteristics analysis), whereas Figures 20 and 21 show the nozzles after the tests with standard diesel fuel and B30 fuel, correspondingly. Though large quantities of carbonaceous deposits could be observed on free surfaces for both fuels, no deposits were found on internal surface of spray holes.

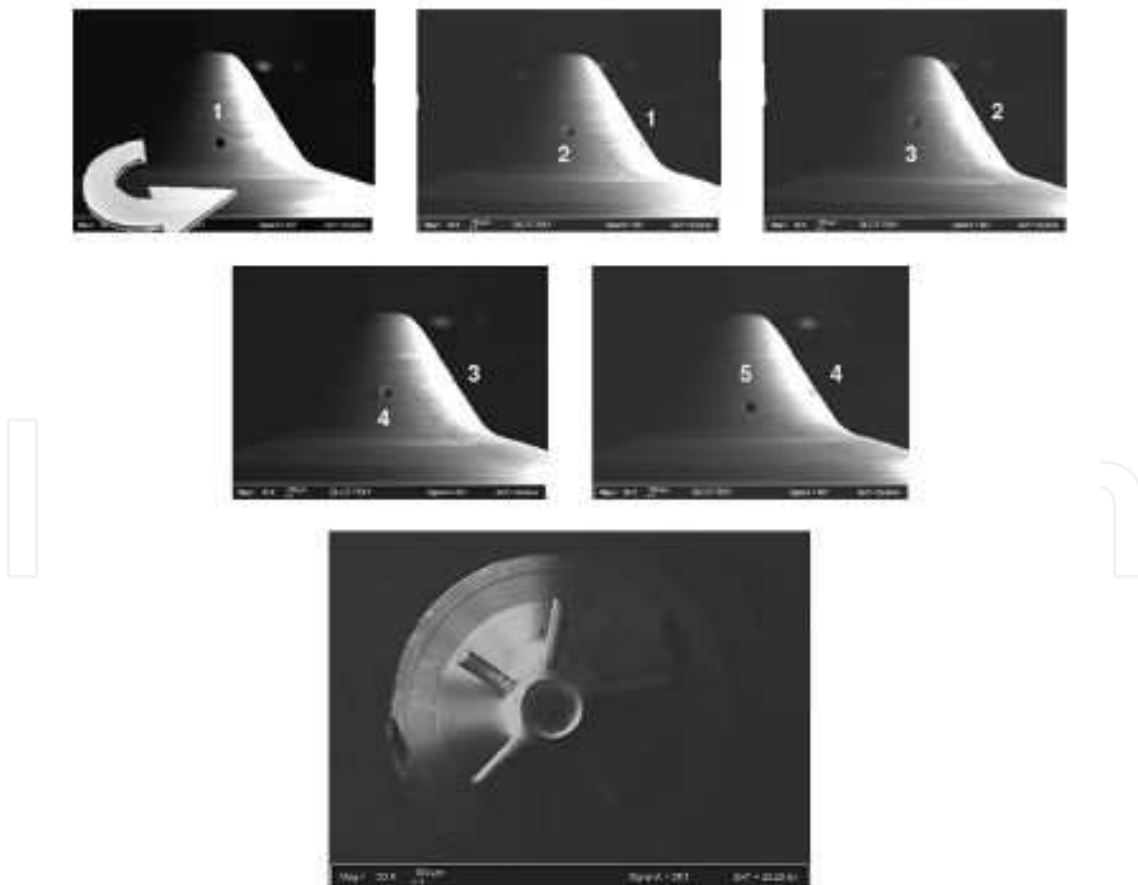


Figure 19. Nozzle body tip and silicon model with labelled holes

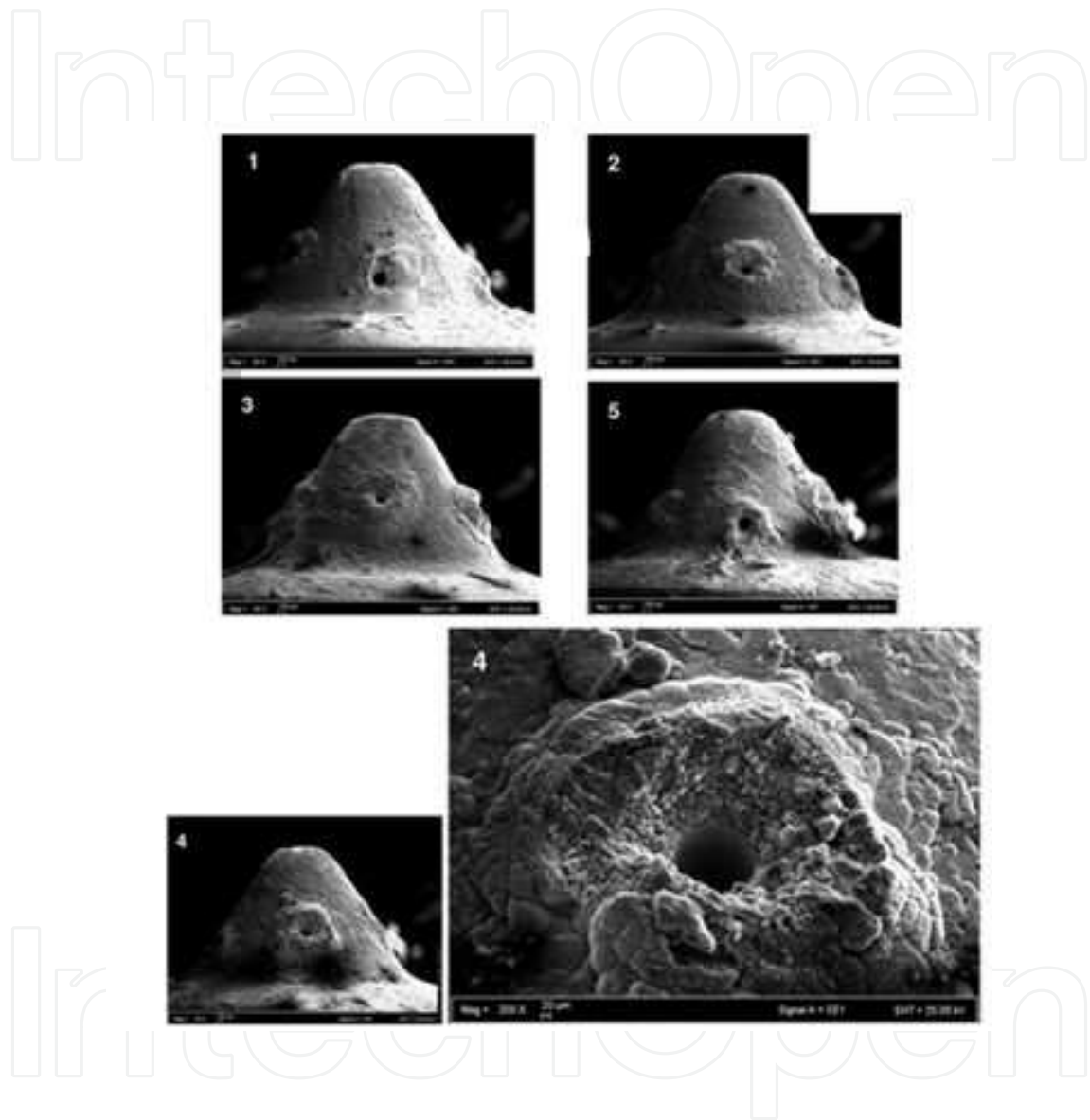


Figure 20. Images of the nozzle after endurance test with standard diesel fuel

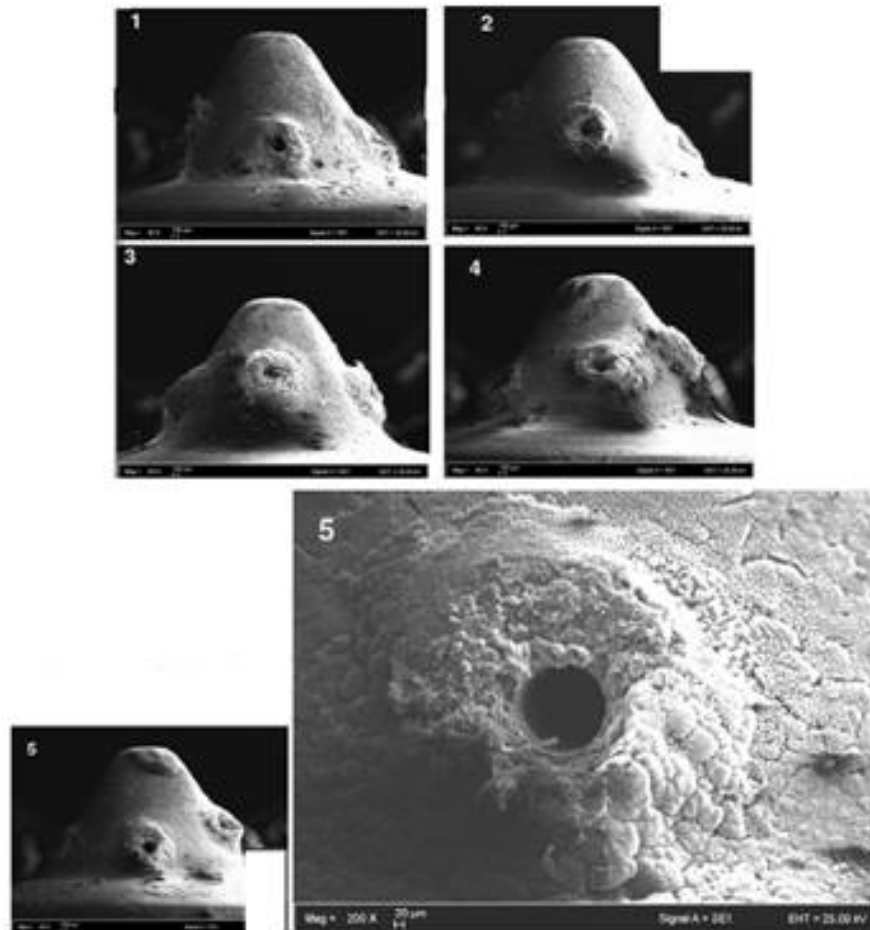


Figure 21. Images of the nozzle after endurance test with B30 fuel

Finally, nozzle deposits were analyzed by Thermal Gravimetric Analysis (TGA), which showed no big difference in deposits composition for the nozzles operated with standard diesel and B30 blend.

4. Conclusions

Fully formulated prototype lubricants based on synthetic esters had low toxicity for aqueous organisms (algae and *Daphnia Magna*) and high biodegradability evaluated by the Manometric Respirometry Method.

Among three developed prototype lubricating oils, SEMO 10 had the best tribological performance which was comparable with that of the reference mineral oil. Further improvement of the tribological properties of this lubricating oil was achieved by additive re-formulation. The developed lubricant, SEMO 36, exceeded the reference mineral oil in tribological performance.

Our findings indicated that, in addition to the rheological properties of the lubricating oil, deposit build-up was an important factor controlling the tribological performance of the oil both in simulation experiments and real two-stroke engines. Two kinds of deposits: carbon soot and transparent sliding lacquer were observed on the engine components after tests. Build-up of a transparent sliding lacquer was especially important in the case of SEMO 36 oil and it was related with considerable reduction both in wear rate and friction coefficient. For SEMO 36, surface chemical analysis of the friction zone showed important changes in surface chemical composition, which was especially marked by increase in carbon and oxygen content. It is evident that formation of the sliding deposits stemmed from tribochemical reactions between the oil components and base material (cast iron and steel). The chemical state of carbon and oxygen atoms on the surface of friction zone should be further investigated for better understanding of these mechanisms.

Tests in real two-stroke engines were performed using mixtures of the developed lubricant with petrol or bioethanol. In both cases, no seizure between piston ring and cylinder liner was observed. When using bioethanol, the engine components were clean without important carbon soot deposits.

Engine power slightly decreased and fuel consumption slightly increased - on a volumetric basis when bioethanol E85 was blended with the newly developed lubricating oil SEMO 36. However, these results might be related with lower calorific value of ethanol as compared with petrol. Besides, the new lubricating oil improved scuffing resistance in combination with miscible lubricants and significantly reduced the environmental impact. In addition to low toxicity and high biodegradability, emissions of CO, NO_x and hydrocarbons from engines lubricated with the newly developed lubricants were lower than with traditional mineral oil and much below the limits established for portable applications.

Concluding, a new generation of lubricating oils for two-stroke engines have been developed combining low friction, good protection against wear and scuffing, no ash residue, low carbon soot or other deposit formation. These lubricating oils are compatible with bioethanol E85.

Application of Cr DLC coating on injection nozzles significantly increased the corrosion resistance and improved behaviour in engine test.

Though Ti-DLC coating also improved substrate corrosion resistance, its performance in engine test was worse than for Cr DLC coating.

Deposit chemical composition and the nozzle performance did not significantly vary in endurance tests when standard diesel was substituted by B30 blend.

Acknowledgements

The authors acknowledge financial support of the European Commission, the project CleanEngine "Advanced technologies for highly efficient Clean Engines working with alternative fuels and lubes" under contract TST5-CT2006-031241, and the Spanish Minister of Science and

Innovation, for co-financing the project under contracts ENE 2008-00652-E/ALT “Tecnologías Avanzadas para motores limpios altamente eficientes, trabajando con combustibles y lubricantes renovables”, RYC-2009-0412 and BIA2011-25653. Also, the authors acknowledge support received from other partners who participated in the projects: ARIZONA Chemical, OBR, GUASCOR Power, BAM, AVL and INSTITUTO MOTORI.

We appreciate the useful help of Olatz Areitioaurtena and Raquel Bayón on performing Biodegradability, toxicity and corrosion characterizations and tests.

Author details

Xana Fernández-Pérez¹, Amaya Igartua¹, Roman Nevshupa², Patricio Zabala³, Borja Zabala³, Rolf Luther⁴, Flavia Gili⁵ and Claudio Genovesio⁶

1 Fundación Tekniker, Avda, Otaola, Eibar, Spain

2 Instituto de Ciencias de la Construcción Eduardo Torroja (IETcc), c/ Serrano Galvache, Madrid, Spain

3 Abamotor Energía, SL, B. Astola, Abadiano, Spain

4 Fuchs Europe GmbH, Mannheim D, Germany

5 CRF StradaTorino Orbassano, Italy

6 FIRAD S.p.A, Fabbrica Italiana Ricambi Apparati Diesel, Bagnolo, Italy

References

- [1] Igartua, A; Barriga, J; Aranzabe, A; (2005) *Biodegradable Lubricants*. Virtual Tribology Institute Edition, ISBN 83-70204-418-X.
- [2] Woydt, M; Skopp, A; (2005) *Ash-free and bionotox engine oils*. In: *Biodegradable lubricants*, eds. A. Igartua, J. Barriga, A. Aranzabe, Radom: Virtual Tribology Institute, Institute of Terotechnology; p. IV.6-IV.9.
- [3] ASTM D-445-06: Standard Test Method for Kinematic Viscosity of Transparent and Opaque Liquids (and Calculation of Dynamic Viscosity).
- [4] ASTM D-2270-04: Standard Practice for Calculating Viscosity Index from Kinematic Viscosity at 40 and 100°C.
- [5] OECD guidelines for testing of chemicals: Section 3; 2003. 12 p.

- [6] OECD 301F: Manometric Respirometry Test. OECD guidelines for testing of chemicals; 1992.
- [7] OECD 201: Alga, Growth Inhibition Test. OECD guidelines for testing of chemicals; 2006.
- [8] OECD 202: Daphnia sp. Acute Immobilisation Test. OECD guidelines for testing of chemicals; 2004.
- [9] DIN 51834-2. Tribological test in the translatory oscillation apparatus. Part 2: Standard Test Method for Measuring the Friction and Wear Properties of EP Lubricating Oils Using the SRV Test Machine; 2004.
- [10] Kostetsky, BI; (1992) *The structural-energetic concept in the theory of friction and wear (synergism and self-organization)*. Wear; 159:1-15.
- [11] Nevshupa, RA ; (2009) *The role of athermal mechanisms in the activation of tribodesorption and triboluminescence in miniature and lightly loaded friction units*. Journal of Friction and Wear; 30:118-126.
- [12] Igartua, A; Nevshupa, R; Fernández-Pérez, X; Conte, M; Zabala, R; Bernaola, J; Zabala, P; Luther, R; Rausch, R; (2011) *Alternative Eco-Friendly Lubes for Clean Two-Stroke Engines*. Tribology International, 44, 727-736.
- [13] Martínez, L; Nevshupa, R; Álvarez, L; Huttel, Y; Méndez, J; Román, E; Mozas, E; Valdés, JR ; Jimenez, MA; Gachon, Y; Heau, C; Faverjon, F; (2009) *Application of diamond-like carbon coatings to elastomers frictional surfaces*. Tribology International, v. 42, pp. 584-590.
- [14] Bayón, R; Nevshupa, R; Zubizarreta, C; Ruiz de Gopegui, U; Barriga, J; Igartua, A; (2010) *Characterisation of tribocorrosion behaviour of multilayer PVD coatings*. Analytical and Bioanalytical Chemistry. V. 396. P. 2855-2862.
- [15] Bayón, R; Zubizarreta, C; Nevshupa, R; Rodriguez, JC; Fernández-Pérez, X; Ruiz de Gopegui, U; Igartua, A; (2011) *Rolling-sliding, scuffing and tribocorrosion behaviour of PVD multilayer coatings for gears application*. Industrial Lubrication and Tribology. V. 63/1. P. 17–26.
- [16] Alajbegovic, A; Meister, G; Greif, D; Basara, B; (2001) *Three Phase Cavitating Flows in High Pressure Swirl Injectors*. 4th Int. Conf. on Multiphase Flow – ICMF'01, May 27 – June 1, 2001, New Orleans, Louisiana, U.S.A.
- [17] Von Berg, E; Alajbegovic, A; Tatschl R; Krüger, C; Michels, U; (2001) *Multiphase Modeling of Diesel Sprays with the Eulerian/Eulerian Approach* (DaimlerChrysler AG), ILASS-Europe 2001, Sept. 2-6, 2001, Zürich, Switzerland
- [18] Von Berg, E; Alajbegovic, A; Greif, D; Poredos, A; Tatschl, R; Winklhofer, E (2002); *Break-up Model for Diesel Jets based on Locally Resolved Flow Field in the Injection Hole*, ILASS-Europe 2002, Sept. 9-11, 2002, Zaragoza, Spain

